The synthesis of rhodium substituted ε-iron oxide exhibiting super high frequency natural resonance

Asuka Namai,[a] Marie Yoshikiyo,[a] Sayaka Umeda,[a] Takayuki Yoshida,[b] Tatsuro Miyazaki,[b] Makoto Nakajima,[c] Keita Yamaguchi,[d] Tohru Suemoto,[d] and Shin-ichi Ohkoshi*[ae]

[a]*Department of Chemistry, School of Science, The University of Tokyo*
7-3-1 Hongo, Bunkyo-ku, Tokyo 113-0033, Japan
[b]*Dowa Electronics Materials Co., Ltd.*
1-3-1 Kaigandori, Minami-ku, Okayama 702-8506, Japan
[c]*Department of Physics, Chiba University*
1-33, Yayoicho, Inage Ward, Chiba-shi, Chiba 263-8522, Japan
[d]*Institute for Solid State Physics, The University of Tokyo*
5-1-5 Kashiwanoha, Kashiwa, Chiba 277-8581, Japan
[e]*CREST, JST, K's Gobancho, 7 Gobancho, Chiyoda-ku, Tokyo 102-0076, Japan*

*Correspondence should be addressed to S. O.
ohkoshi@chem.s.u-tokyo.ac.jp

Contents:

§ 1. Synthesis

Table S1. Rhodium concentration in the synthesis and the observed concentration by ICP-MS measurement.

Sample		1	2	3	4	5	6	7	8	9
Rh/(Fe+Rh)	feed	0.0	0.02	0.04	0.06	0.08	0.10	0.13	0.15	0.18
	obs.	0.0	0.02	0.04	0.06	0.07	0.10	0.11	0.14	0.16

§ 2. Investigation of the sintering temperature

In order to investigate the appropriate sintering temperature to obtain the ε-phase, we attempted various sintering temperatures in the range of 1020~1300 ºC. The Rietveld analyses of XRD patterns indicated that the sample sintered at 1080 ºC had a high ε-phase ratio, and hence, we adopted 1080 ºC as the sintering temperature.

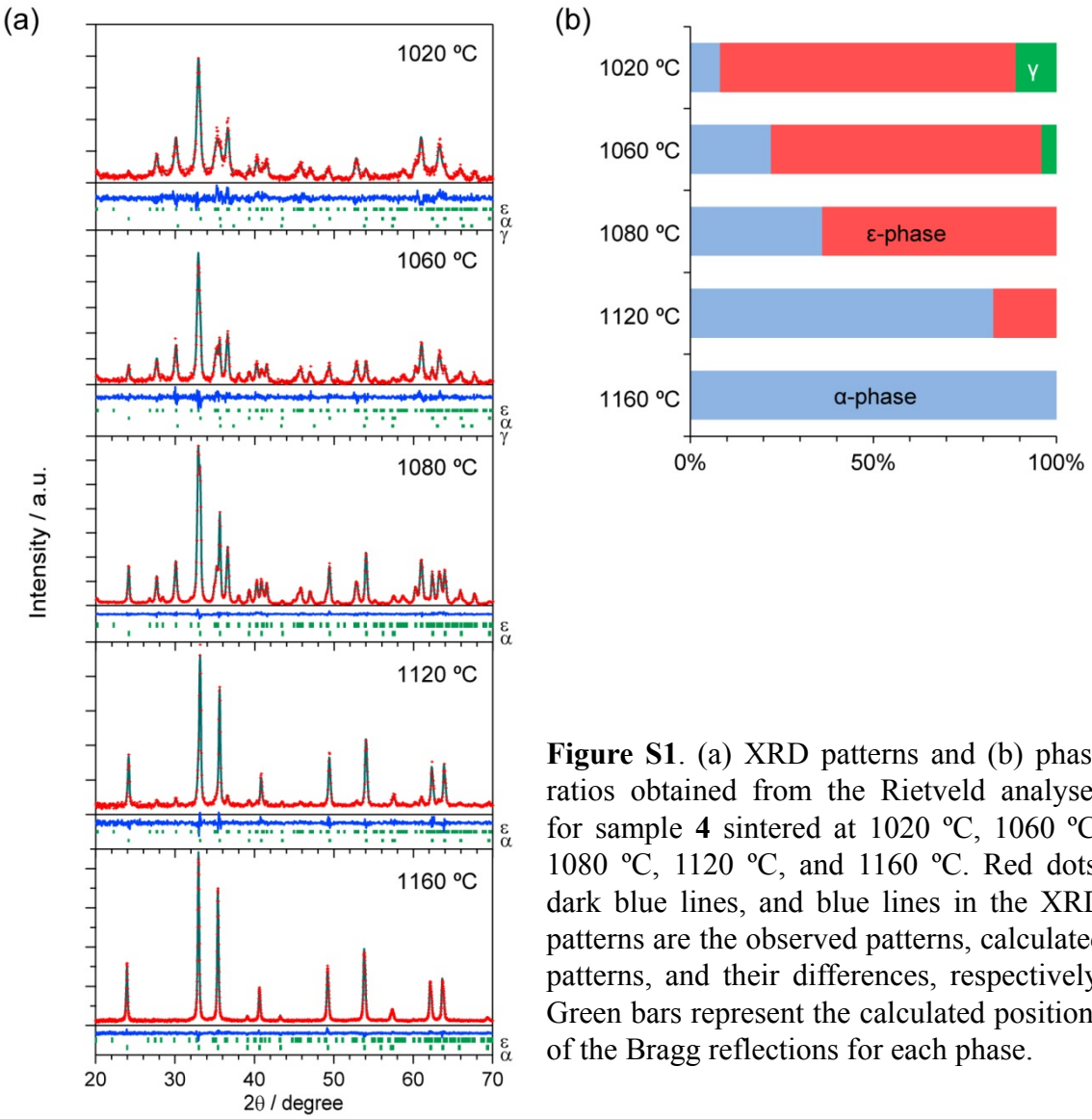

Figure S1. (a) XRD patterns and (b) phase ratios obtained from the Rietveld analyses for sample **4** sintered at 1020 ºC, 1060 ºC, 1080 ºC, 1120 ºC, and 1160 ºC. Red dots, dark blue lines, and blue lines in the XRD patterns are the observed patterns, calculated patterns, and their differences, respectively. Green bars represent the calculated positions of the Bragg reflections for each phase.

§ 3. TEM study

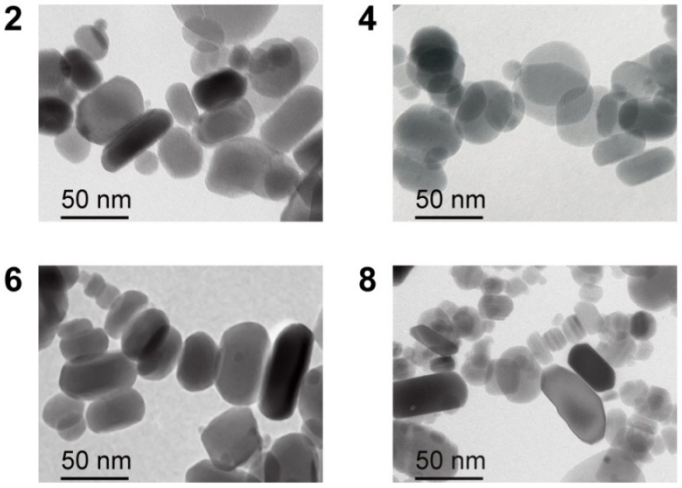

Figure S2. TEM images for samples **2**, **4**, **6**, and **8**.

Table S2. Particle size and aspect ratio of obtained from TEM images.

Sample	Long axis	Short axis	Average aspect ratio
1	33±15 nm	24±11 nm	1.4
2	35±16 nm	25±11 nm	1.4
3	36±17 nm	26±12 nm	1.4
4	35±16 nm	27±12 nm	1.3
5	36±18 nm	27±14 nm	1.3
6	29±17 nm	21±13 nm	1.5
7	27±18 nm	19±12 nm	1.5
8	23±14 nm	16± 9 nm	1.5
9	22±13 nm	16± 9 nm	1.4

§ 4. Crystal structure analyses

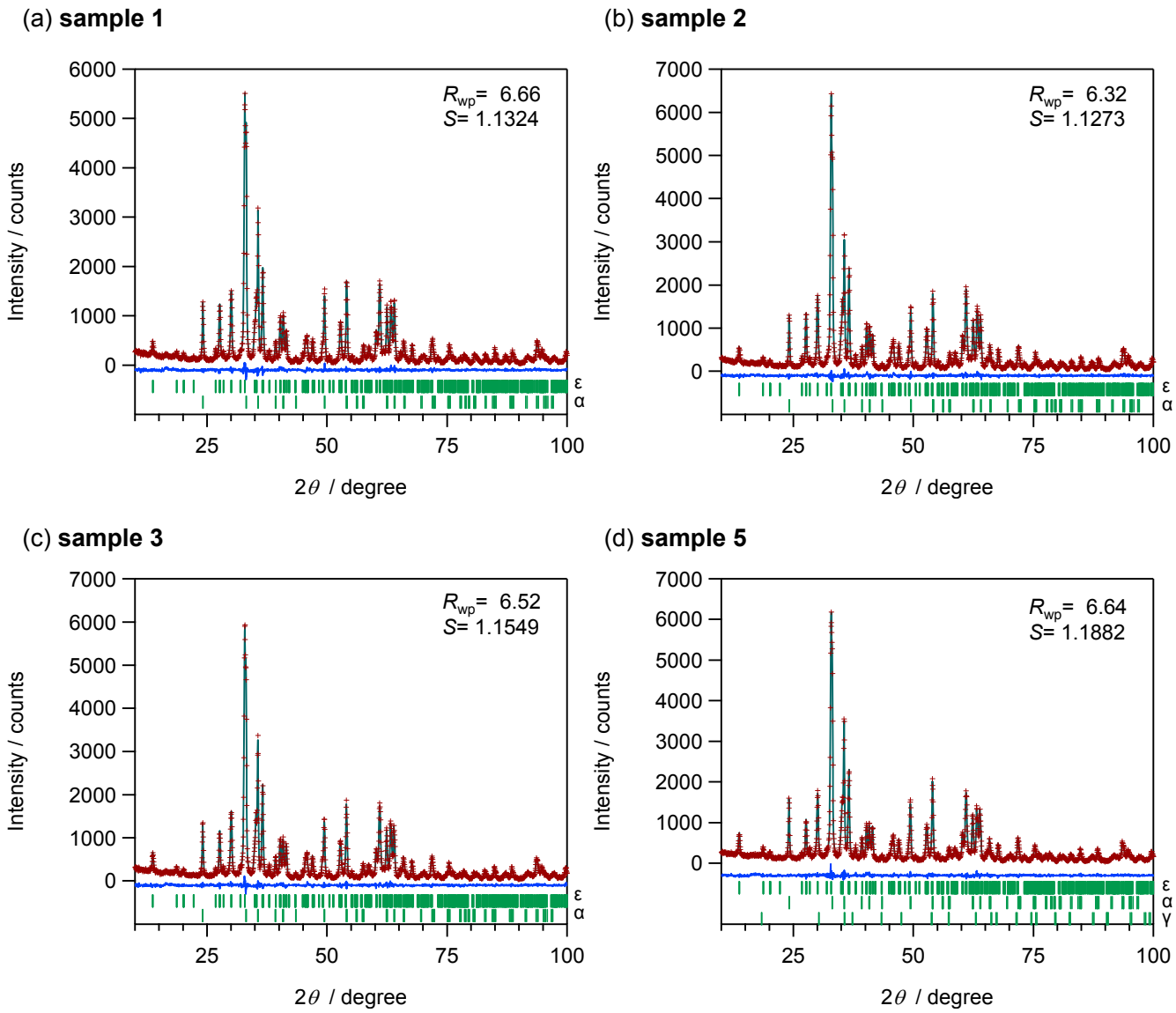

Figure S3. XRD patterns and Rietveld analyses for samples **1**−**3**, **5**. Red dots, dark blue lines, and blue lines are the observed patterns, calculated patterns, and their differences, respectively. Green bars represent the calculated positions of the Bragg reflections for each phase.

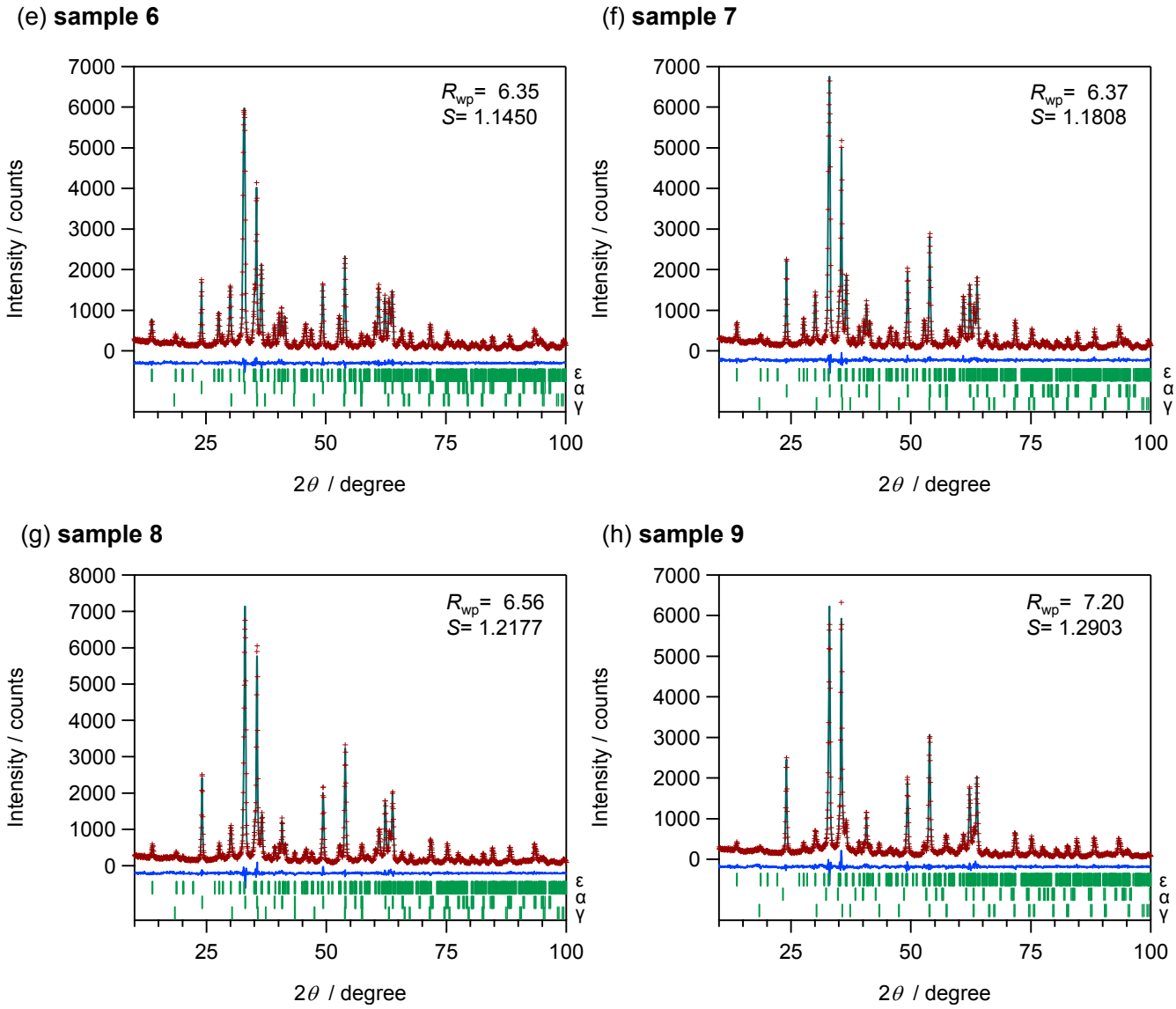

Figure S4. XRD patterns and Rietveld analyses for samples **6**–**9**. Red dots, dark blue lines, and blue lines are the observed patterns, calculated patterns, and their differences, respectively. Green bars represent the calculated positions of the Bragg reflections for each phase.

The synthesis and characterization of pure α-$Rh_xFe_{2-x}O_3$ nanoparticles for crystal structure analysis

α-$Rh_xFe_{2-x}O_3$ nanoparticles (x= 0, 0.12, 0.30, and 0.36) were prepared by sintering the precursors at 1180 ºC (x= 0), 1160 ºC (x= 0.12), and 1140ºC (x= 0.30, 0.36) for 4 hours in air. The SiO_2 matrix was etched by stirring in a NaOH solution for 24 hours at 60 ºC.

Table S3. Rhodium concentration in the synthesis and the observed concentration by ICP-MS measurement.

Sample		x= 0	x= 0.12	x= 0.30	x= 0.36
Rh/(Fe+Rh)	feed	0.0	0.06	0.18	0.20
	obs.	0.0	0.06	0.15	0.18

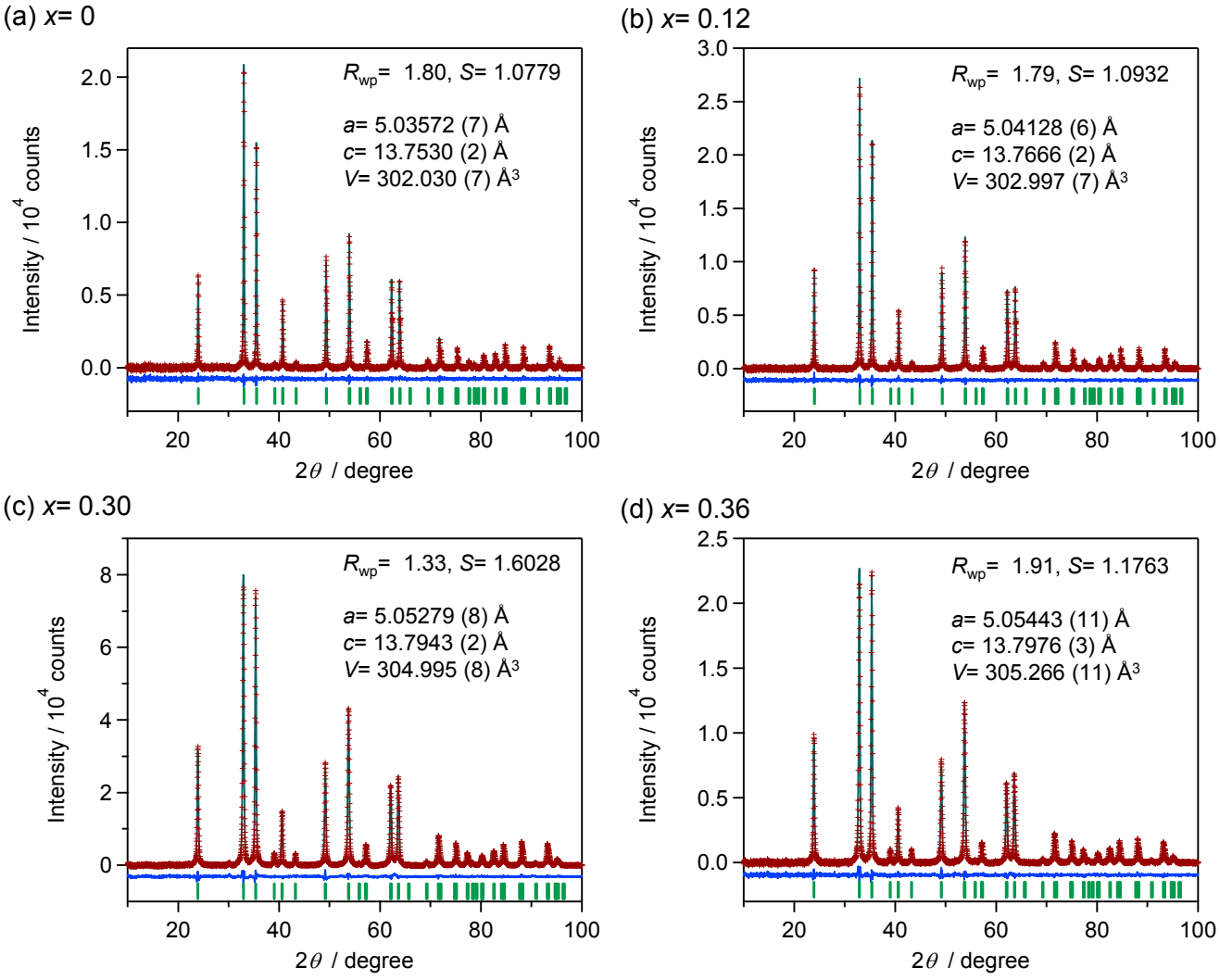

Figure S5. XRD patterns and Rietveld analyses for α-$Rh_xFe_{2-x}O_3$ (x= 0, 0.12, 0.30, 0.36). Red dots, dark blue lines, and blue lines are the observed patterns, calculated patterns, and their differences, respectively. Green bars represent the calculated positions of the Bragg reflections.

α-$Rh_xFe_{2-x}O_3$

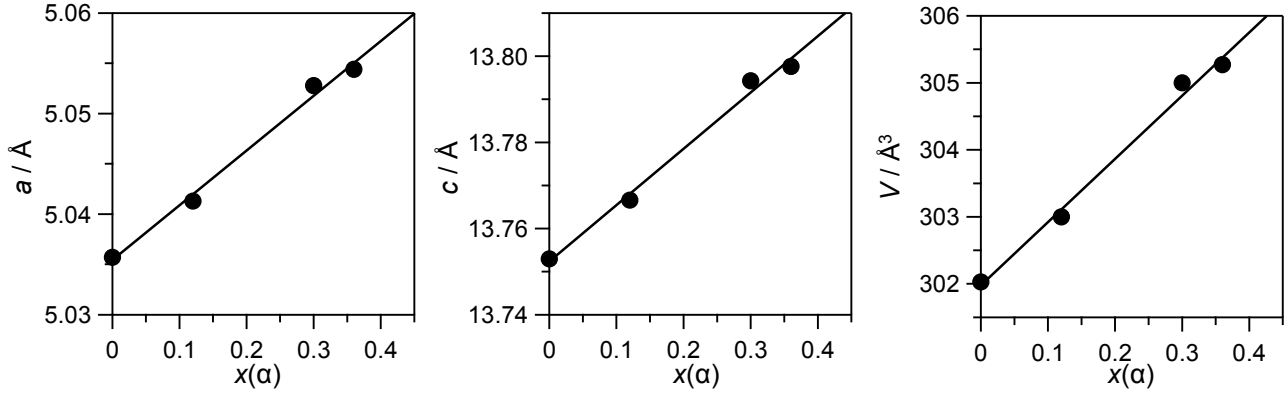

Figure S6. Lattice constants (*a*, *c*) and lattice volume (*V*) *versus* *x*(α) value plots for pure α-$Rh_xFe_{2-x}O_3$ samples (*x*= 0, 0.12, 0.30, and 0.36).

ε-$Rh_xFe_{2-x}O_3$

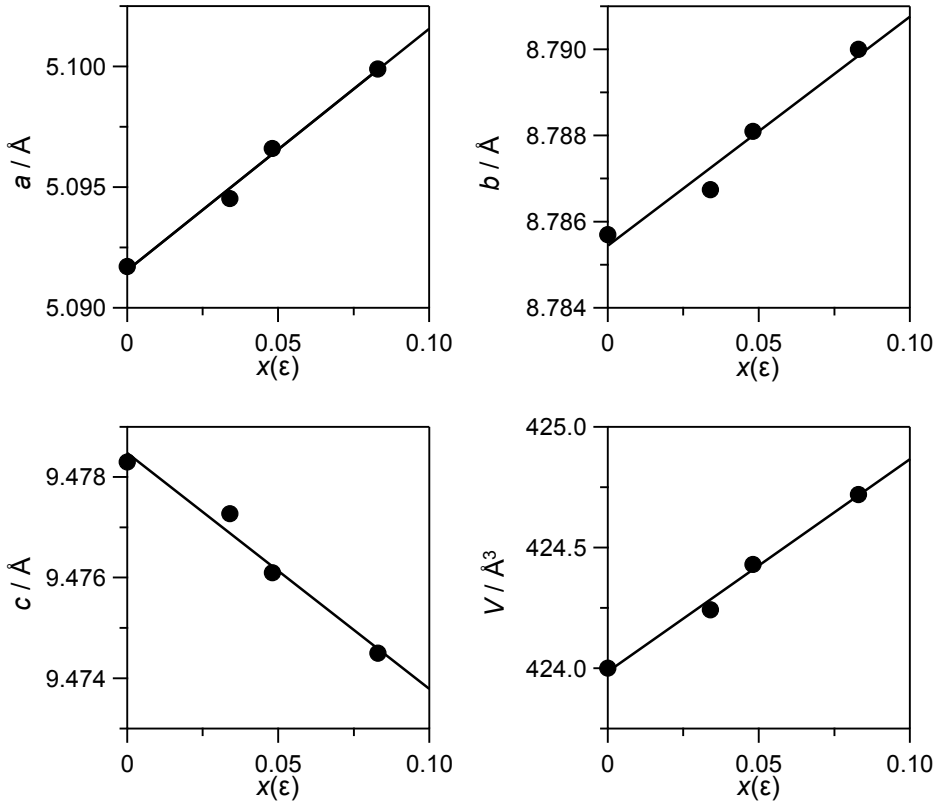

Figure S7. Lattice constants (*a*, *b*, *c*) and lattice volume (*V*) *versus* *x*(ε) value plots for ε-$Rh_xFe_{2-x}O_3$ for samples **1**, **2**, **3**, and **4**.

Table S4. Crystal structure parameters of ε-$Rh_xFe_{2-x}O_3$ for samples **1**–**5** refined by Rietveld analyses of the XRD patterns.

Sample		**1**	**2**	**3**	**4**	**5**
		ε-Fe_2O_3	ε-$Rh_{0.03}Fe_{1.97}O_3$	ε-$Rh_{0.05}Fe_{1.95}O_3$	ε-$Rh_{0.08}Fe_{1.92}O_3$	ε-$Rh_{0.10}Fe_{1.90}O_3$
W_ε / wt%		64	68	67	64	64
a / Å		5.0917 (3)	5.0945 (3)	5.0966 (3)	5.0999 (3)	5.1020 (3)
b / Å		8.7857 (5)	8.7867 (5)	8.7881 (5)	8.7900 (5)	8.7906 (5)
c / Å		9.4783 (7)	9.4773 (7)	9.4761 (8)	9.4745 (7)	9.4735 (8)
V / Å^3		424.00 (5)	424.24 (5)	424.43 (5)	424.72 (5)	424.88 (5)
Rh	A	0	0	0	0	0
occupancy	B	0	0 (0)	0 (0)	0 (0)	0 (0)
/%	C	0	6 (0)	11 (0)	17 (0)	21 (0)
	D	0	0	0	0	0
Fe_A	*x*	0.315 (2)	0.311 (2)	0.314 (2)	0.308 (2)	0.312 (2)
	y	0.3465 (14)	0.3471 (15)	0.346 (2)	0.3441 (9)	0.347 (2)
	z	0.156 (2)	0.159 (2)	0.156 (2)	0.161 (2)	0.157 (3)
Fe_B	*x*	0.3169 (11)	0.3207 (10)	0.3207 (12)	0.3213 (12)	0.3198 (12)
	y	0.0324 (5)	0.0328 (4)	0.0324 (5)	0.0324 (4)	0.0318 (5)
	z	0.368 (2)	0.373 (2)	0.371 (3)	0.376 (2)	0.372 (3)
Fe_C	*x*	0.3056 (11)	0.3098 (9)	0.3081 (10)	0.3120 (9)	0.3127 (9)
	y	0.6582 (6)	0.6579 (5)	0.6595 (6)	0.6589 (5)	0.6592 (6)
	z	0.378 (3)	0.384 (2)	0.380 (2)	0.386 (2)	0.382 (3)
Fe_D	*x*	0.192 (2)	0.190 (2)	0.189 (2)	0.184 (2)	0.189 (2)
	y	0.8495 (13)	0.8490 (13)	0.8492 (14)	0.8524 (8)	0.849 (2)
	z	0.073 (2)	0.076 (2)	0.074 (2)	0.079 (2)	0.074 (3)
O1	*x*	0.025 (5)	0.020 (5)	0.025 (5)	0.026 (5)	0.029 (6)
	y	0.328 (2)	0.329 (2)	0.332 (2)	0.334 (2)	0.328 (3)
	z	0	0	0	0	0
O2	*x*	0.995 (5)	0.994 (4)	0.994 (5)	0.992 (5)	0.993 (5)
	y	0.009 (2)	0.007 (2)	0.009 (2)	0.007 (2)	0.007 (3)
	z	0.997 (6)	1.005 (6)	0.999 (6)	1.009 (5)	1.008 (6)
O3	*x*	0.027 (5)	0.023 (5)	0.024 (5)	0.016 (6)	0.021 (6)
	y	0.665 (2)	0.670 (2)	0.667 (2)	0.669 (2)	0.667 (3)
	z	0.013 (3)	0.019 (3)	0.016 (3)	0.020 (3)	0.015 (3)
O4	*x*	0.149 (5)	0.151 (4)	0.149 (5)	0.154 (5)	0.146 (5)
	y	0.494 (2)	0.494 (2)	0.494 (2)	0.492 (2)	0.494 (2)
	z	0.270 (3)	0.275 (2)	0.273 (3)	0.277 (2)	0.273 (3)
O5	*x*	0.152 (5)	0.155 (5)	0.154 (6)	0.148 (5)	0.155 (6)
	y	0.839 (3)	0.837 (2)	0.835 (3)	0.838 (3)	0.841 (3)
	z	0.271 (2)	0.274 (2)	0.274 (2)	0.275 (2)	0.272 (3)
O6	*x*	0.155 (6)	0.153 (6)	0.160 (7)	0.157 (6)	0.158 (7)
	y	0.172 (3)	0.174 (3)	0.174 (3)	0.173 (3)	0.172 (3)
	z	0.242 (3)	0.247 (2)	0.246 (3)	0.249 (2)	0.247 (3)

Table S5. Crystal structure parameters of ε-$Rh_xFe_{2-x}O_3$ for samples **6–9** refined by Rietveld analyses of the XRD patterns.

		6	**7**	**8**	**9**
		ε-$Rh_{0.14}Fe_{1.86}O_3$	ε-$Rh_{0.15}Fe_{1.85}O_3$	ε-$Rh_{0.18}Fe_{1.82}O_3$	ε-$Rh_{0.19}Fe_{1.81}O_3$
W_ε / wt%		59	49	37	24
a / Å		5.1055 (3)	5.1067 (4)	5.1095 (5)	5.1110 (9)
b / Å		8.7941 (6)	8.7932 (7)	8.7951 (9)	8.798 (2)
c / Å		9.4734 (9)	9.4699 (11)	9.471 (2)	9.472 (3)
V / Å^3		425.34 (6)	425.24 (7)	425.59 (10)	425.9 (2)
Rh	A	0 (1)	0 (1)	2 (2)	3 (3)
occupancy	B	2 (1)	2 (1)	2 (3)	5 (4)
/%	C	26 (1)	29 (1)	32 (2)	31 (3)
	D	0	0	0	0
Fe_A	*x*	0.313 (3)	0.319 (3)	0.311 (4)	0.316 (7)
	y	0.3429 (11)	0.351 (2)	0.3379 (15)	0.338 (3)
	z	0.161 (2)	0.168 (3)	0.165 (4)	0.158 (9)
Fe_B	*x*	0.3244 (13)	0.324 (2)	0.325 (3)	0.321 (5)
	y	0.0316 (5)	0.0321 (7)	0.0308 (10)	0.028 (2)
	z	0.377 (3)	0.381 (3)	0.381 (5)	0.374 (10)
Fe_C	*x*	0.3144 (10)	0.3129 (12)	0.318 (2)	0.319 (3)
	y	0.6580 (6)	0.6598 (9)	0.6573 (13)	0.656 (2)
	z	0.386 (2)	0.394 (3)	0.388 (4)	0.381 (9)
Fe_D	*x*	0.191 (2)	0.195 (2)	0.196 (4)	0.205 (5)
	y	0.8520 (10)	0.842 (2)	0.8546 (13)	0.858 (2)
	z	0.077 (3)	0.085 (3)	0.078 (4)	0.066 (10)
O1	*x*	0.021 (7)	0.019 (10)	0.023 (12)	0.05 (2)
	y	0.327 (3)	0.332 (5)	0.328 (5)	0.318 (9)
	z	0	0	0	0
O2	*x*	0.988 (6)	0.997 (8)	0.978 (10)	0.98 (2)
	y	0.006 (3)	0.006 (4)	0.006 (4)	0.005 (8)
	z	1.008 (6)	1.019 (7)	1.013 (9)	1.01 (2)
O3	*x*	0.019 (7)	0.008 (10)	0.004 (12)	0.01 (2)
	y	0.670 (3)	0.671 (5)	0.664 (5)	0.655 (9)
	z	0.026 (4)	0.028 (4)	0.029 (7)	0.017 (14)
O4	*x*	0.161 (6)	0.158 (8)	0.165 (12)	0.15 (2)
	y	0.490 (3)	0.490 (3)	0.496 (5)	0.498 (10)
	z	0.277 (3)	0.283 (3)	0.286 (5)	0.282 (10)
O5	*x*	0.156 (7)	0.163 (9)	0.151 (11)	0.15 (2)
	y	0.836 (4)	0.838 (5)	0.841 (8)	0.830 (12)
	z	0.277 (3)	0.282 (3)	0.277 (5)	0.267 (10)
O6	*x*	0.158 (7)	0.157 (10)	0.160 (13)	0.16 (2)
	y	0.168 (4)	0.171 (4)	0.166 (8)	0.153 (13)
	z	0.250 (3)	0.260 (3)	0.267 (5)	0.278 (11)

Table S6. Crystal structure parameters of α-$Rh_xFe_{2-x}O_3$ for each sample refined by Rietveld analyses of the XRD patterns.

sample		**1**	**2**	**3**	**4**	**5**
		α-Fe_2O_3	α-$Rh_{0.05}Fe_{1.95}O_3$	α-$Rh_{0.12}Fe_{1.88}O_3$	α-$Rh_{0.16}Fe_{1.84}O_3$	α-$Rh_{0.20}Fe_{1.80}O_3$
W_α / wt%		36	32	33	36	34
a / Å		5.0365 (3)	5.0379 (4)	5.0413 (3)	5.0437 (3)	5.0457 (3)
c / Å		13.7554 (9)	13.7589 (9)	13.7668 (9)	13.7729 (8)	13.7762 (9)
V / Å^3		302.18 (4)	302.43 (4)	303.01 (4)	303.43 (3)	303.74 (3)
Fe/Rh	*x*	0	0	0	0	0
	y	0	0	0	0	0
	z	0.14493 (10)	0.14544 (10)	0.14600 (10)	0.14651 (9)	0.14705 (11)
O	*x*	0.3084 (9)	0.3088 (9)	0.3088 (10)	0.3093 (9)	0.3071 (10)
	y	0	0	0	0	0
	z	1/4	1/4	1/4	1/4	1/4

sample		**6**	**7**	**8**	**9**
		α-$Rh_{0.26}Fe_{1.74}O_3$	α-$Rh_{0.28}Fe_{1.72}O_3$	α-$Rh_{0.35}Fe_{1.65}O_3$	α-$Rh_{0.38}Fe_{1.62}O_3$
W_α / wt%		38	47	54	60
a / Å		5.0493 (3)	5.0503 (3)	5.0540 (3)	5.0559 (3)
c / Å		13.7862 (9)	13.7868 (8)	13.7959 (8)	13.8008 (10)
V / Å^3		304.39 (3)	304.53 (3)	305.18 (3)	305.52 (3)
Fe/Rh	*x*	0	0	0	0
	y	0	0	0	0
	z	0.14763 (9)	0.14786 (9)	0.14853 (8)	0.14860 (10)
O	*x*	0.3128 (9)	0.3076 (8)	0.3128 (9)	0.3071 (9)
	y	0	0	0	0
	z	1/4	1/4	1/4	1/4

Table S7. Crystal structure parameters of γ-$Rh_xFe_{2-x}O_3$ for each sample refined by Rietveld analyses of the XRD patterns.

sample		**5**	**6**	**7**	**8**	**9**
		γ-$Rh_{0.5}Fe_{1.5}O_3$	γ-$Rh_{0.4}Fe_{1.6}O_3$	γ-$Rh_{0.4}Fe_{1.6}O_3$	γ-$Rh_{0.3}Fe_{1.7}O_3$	γ-$Rh_{0.3}Fe_{1.7}O_3$
W_γ / wt%		1	3	5	8	15
a / Å		8.35 (2)	8.349 (8)	8.343 (5)	8.347 (4)	8.343 (6)
V / Å^3		582 (2)	582.0 (9)	580.7 (6)	581.5 (5)	580.6 (7)
Fe_A	*x*	0	0	0	0	0
	y	0	0	0	0	0
	z	0	0	0	0	0
Fe_B	*x*	5/8	5/8	5/8	5/8	5/8
	y	5/8	5/8	5/8	5/8	5/8
	z	5/8	5/8	5/8	5/8	5/8
O	*x*	3/8	3/8	3/8	3/8	3/8
	y	3/8	3/8	3/8	3/8	3/8
	z	3/8	3/8	3/8	3/8	3/8

§ 5. Magnetic properties

FCM curves

To investigate the magnetic properties of ε-phase excluding the contribution of α- and γ-phases, the FCM curves were calibrated by using the observed curve of pure α-$Rh_xFe_{2-x}O_3$ and the estimated curves of γ-$Rh_xFe_{2-x}O_3$ based on Bloch law.

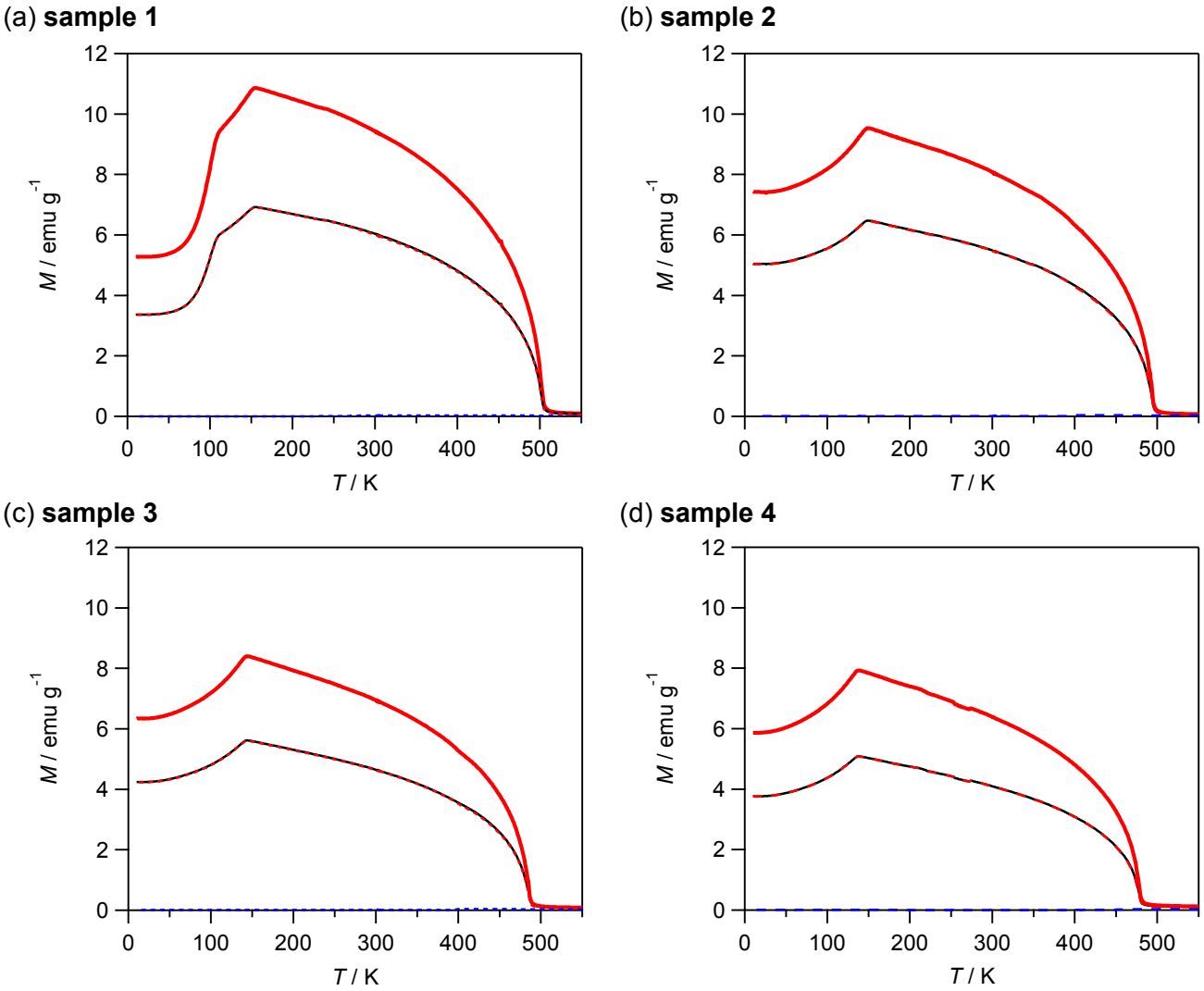

Figure S8. Measured and calibrated FCM curves in an external field of 1 kOe for samples **1**–**4**. Black lines indicate the measured curves, whereas dotted red, blue, and gray lines represent the estimated components of ε-phase, α-phase, and γ-phase, respectively. The bold red lines represent the calibrated curves for ε-$Rh_xFe_{2-x}O_3$.

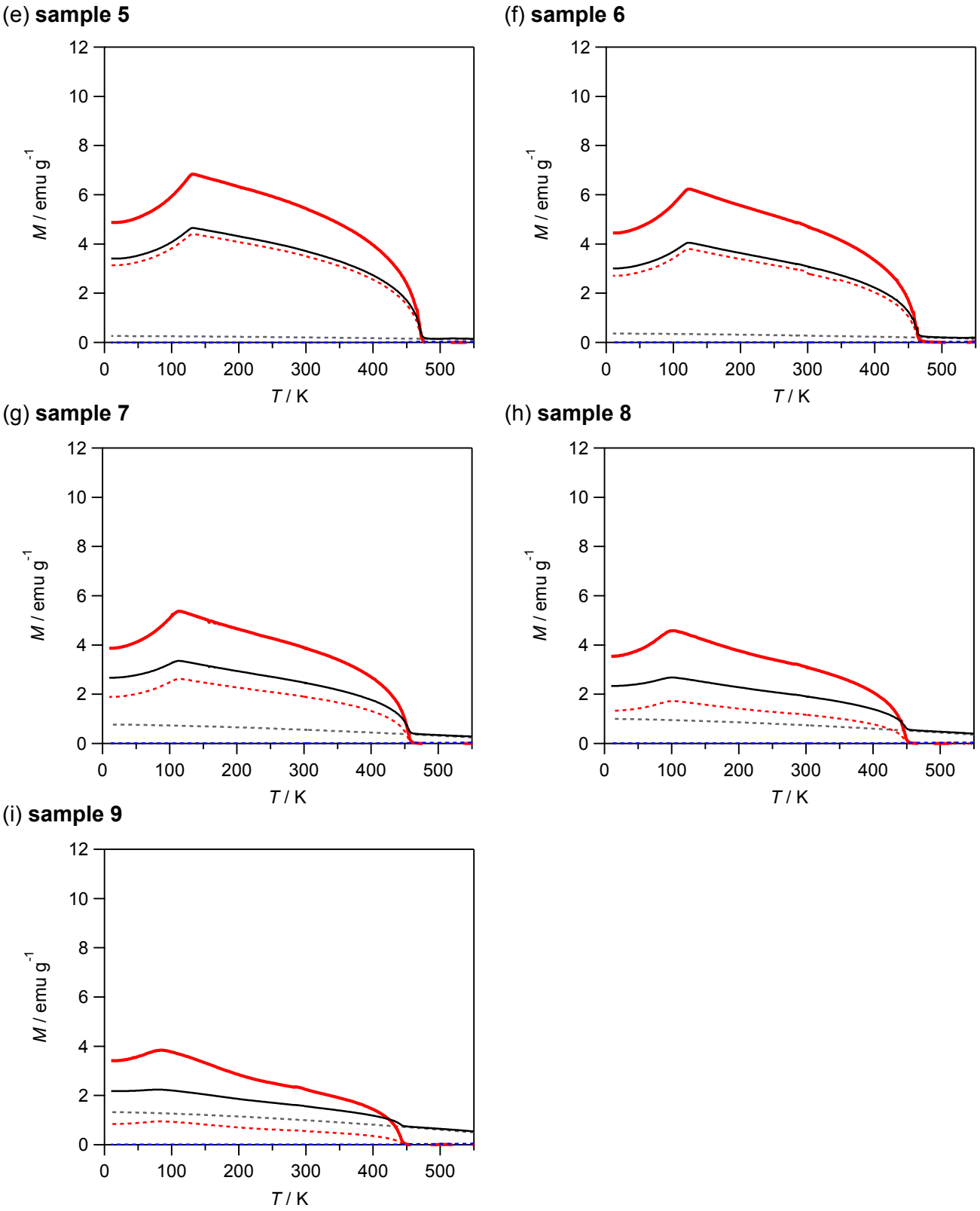

Figure S9. Measured and calibrated FCM curves in an external field of 1 kOe for samples **5**–**9**. Black lines indicate the measured curves, whereas dotted red, blue, and gray lines represent the estimated components of ε-phase, α-phase, and γ-phase, respectively. The bold red lines represent the calibrated curves for ε-$Rh_xFe_{2-x}O_3$.

M-H curves

To investigate the magnetic properties of ε-phase excluding the contribution of α- and γ-phases, the *M-H* curves were calibrated by using the observed curve of pure α-$Rh_xFe_{2-x}O_3$ and the estimated curves of γ-$Rh_xFe_{2-x}O_3$ based on Langevin function.

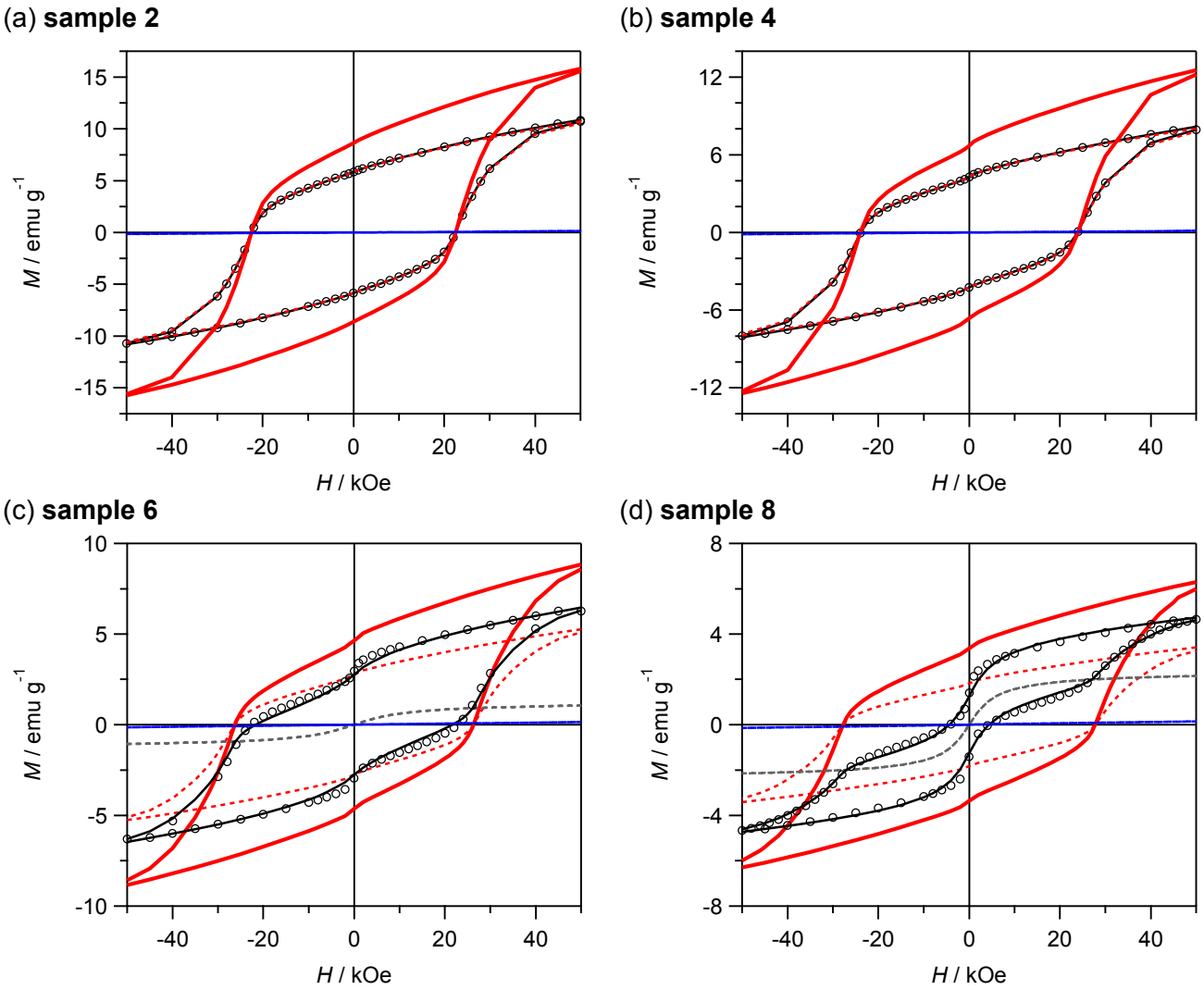

Figure S10. Magnetization *versus* external magnetic field curves at 300 K for samples **2**, **4**, **6** and **8**. Open circle is the observed value. Dotted lines represent contributions from each phase (red, blue, and gray dotted lines represent the ε-, α-, and γ-phases, respectively). Black solid line is their sum. Red solid line denotes the estimated value for a single-phase ε-$Rh_xFe_{2-x}O_3$.